Transportation Geotechnics 45 (2024) 101193

Contents lists available at ScienceDirect

Transportation Geotechnics

journal homepage: www.elsevier.com/locate/trgeo

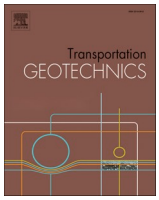

The effect of ballast moisture content and fouling index on railway track settlement

C. Charoenwong [a,*], D.P. Connolly [a,*], P. Alves Costa [b], P. Galvín [c,d], A. Romero [c]

[a] Institute for High Speed Rail and Systems Integration, School of Civil Engineering, University of Leeds, UK
[b] CONSTRUCT-FEUP, Department of Civil Engineering, Faculty of Engineering, University of Porto, Rua Dr. Roberto Frias s/n, 4200-465 Porto, Portugal
[c] Escuela Técnica Superior de Ingeniería, Universidad de Sevilla, Camino de los Descubrimientos s/n, 41092 Sevilla, Spain
[d] Laboratory of Engineering for Energy and Environmental Sustainability, Universidad de Sevilla, Camino de los Descubrimientos s/n, 41092 Sevilla, Spain

ARTICLE INFO

Keywords:
Railway ballast fouling index
Moisture content of fines
Differential track settlement
Railway track geometry
Climate change
Earthwork stiffness

ABSTRACT

A primary function of railway ballast is to maintain vertical track geometry, however over time it becomes contaminated with fines which reduce its ability to free-drain. Then, in the presence of moisture, the individual particles have greater scope for rearrangement thus leading to increased track settlement. This behaviour has received limited studied from a differential settlement viewpoint despite track geometry being the dominant metric used for scheduling railway maintenance. Therefore this paper presents a novel numerical modelling approach capable of simulating the effect of ballast fouling and moisture content on the evolution of track geometry. First the model is presented, which uses a 2.5D finite element approach with perfectly matched layers to simulate static and dynamic stress fields from trains. Non-linear track-soil effects are considered and loading is applied using a multi-body vehicle with train-track coupling. Differential track settlement is calculated in an iterative manner, being updated after every train passage. It is used to perform four analyses, the first of which is to investigate the effect of ballast fouling considering dry conditions. Next the effect of moisture of fines is studied. Then, the effect of earthwork stiffness and train speed is analysed. It is shown that elevated levels of ballast fouling lead to faster deterioration in track geometry, particularly in the presence of moisture. When the ballast is heavily fouled and the moisture of fines is high, rapid deterioration occurs. In contrast, when the ballast is kept dry, the increase in degradation rate for fouled ballast is limited. Higher train speeds and lower earthwork stiffness's make this effect more pronounced.

Introduction

Under repeated train loading railway tracks undergo plastic deformation. This deterioration is not distributed uniformly along the track but instead varies along each section. Deterioration in vertical track geometry leads to a cycle where train-track dynamic interaction forces increase, resulting in further track degradation. These longitudinal track irregularities evolve with each load passage. Consequently, the characteristics of the train-track dynamic interaction forces, track stress distributions, and settlements change over time. The track geometry profile is the most commonly used factor in determining the scheduling of track maintenance operations.

During initial construction and track renewals, fresh ballast containing clean, uniformly graded coarse aggregate is incorporated into the track substructure. However, over time, the new ballast deteriorates and/or becomes contaminated. This contamination is for example due to aggregate breakage, which results in the presence of an increased percentage of smaller ballast particles in the matrix. It can also occur from below (e.g. mud pumping) and above (e.g. coal from freight wagons). Regardless, these contaminates are known as fouling and effect the particle size distribution of the ballast layer. Ballast fouling can result in track geometry issues, for example inadequate drainage, increased settlement and reduced lateral track stability.

One crucial role of the ballast is to facilitate effective drainage. However, as becomes fouled, it loses its ability to free-drain. Over the past few decades, extensive research has been conducted to explore the performance of unbound aggregate materials under various moisture conditions [17,29]. Even in the case of clean aggregate materials, moisture can introduce lubrication between particle contacts, resulting in heightened deformation and reduced strength [36]. This effect

* Corresponding authors.
E-mail addresses: cncc@leeds.ac.uk (C. Charoenwong), d.connolly@leeds.ac.uk (D.P. Connolly).

https://doi.org/10.1016/j.trgeo.2024.101193
Received 12 December 2023; Received in revised form 15 January 2024; Accepted 24 January 2024
Available online 29 January 2024

becomes more pronounced as the moisture of fines (w) rises, particularly as it approaches saturation [24].

To quantify fouling, Selig & Waters [33] proposed the use of a Fouling Index (FI), which is calculated as the sum of the percentage by weight of ballast sample passing the 4.75 mm (No. 4) sieve and the percentage passing the 0.075 mm (No. 200) sieve. This index serves to quantify ballast fouling conditions and estimate the drainage performance of wet fouled ballast.

To predict differential track settlement due to train loading, various methodologies have been proposed by de Miguel et al. [12], Grossoni et al. [15], Kumar et al. [22] and Nielsen & Li [30]. These methods use iterative simulations of train passages along with settlement models to assess differential track settlement, taking into account variations in track geometry. However, the complexities arise when trying to simulate cyclic loading over time. Accurately representing the 3D dynamic stress fields in the track and the ground beneath it, particularly over numerous loading cycles, tends to require significant computational resources [6,7,9,14].

A railway settlement prediction model primarily hinges on evaluating the stress/strain behaviour of the infrastructure and then determining the subsequent settlement. When it comes to predicting settlement, the prevalent methods are either constitutive, as detailed by Dahlberg [11] and Guo et al. [16] and Shih et al. [35], or empirical, as demonstrated by Indraratna & Nimbalkar [18] and Li & Selig [27,28] among others. The constitutive methodology, while thorough, tends to be resource-intensive in terms of computation and necessitates a detailed set of material inputs, complicating its real-world implementation, as outlined by Chen & McDowell [5] and Shan et al. [34]. On the other hand, empirical models, characterised by their limited number of parameters and computational efficiency, can accurately replicate on-track settlement behaviour when applied judiciously[32].

In this paper, a novel empirical equation for ballast settlement, derived from laboratory data on degraded ballast exposed to both dry and wet conditions, is presented. The proposed settlement equation is integrated with a new numerical algorithm for computing differential track settlement in ballasted tracks under various fouling conditions. Train-track interaction, vehicle dynamics, and the propagation of 3D stress fields are all explicitly modelled. The computational implementation is high, even when using solid elements to represent 3D stress fields. An equivalent-linear wavenumber finite element method combined with empirical settlement relationships is employed. This combination allows track irregularities to evolve after each load passage before applying the subsequent load. Four different case studies are examined. The first case investigates the impact of Fouling Index (FI) under dry subgrade conditions, with FI values ranging from 5 to 40. The second case studies the influence of moisture of fines on fouled ballast, exploring moisture levels of 3 %, 6 %, and 9 % (w) at a constant FI value of 40. The third case examines the effect of a reduced embankment stiffness considering different levels of ballast FI and moisture content. The final case assesses the effect of linespeed under various ballast conditions, considering speeds of 100, 150, and 200 km/h.

Differential settlement modelling

Model overview

A two-step coupled modelling strategy is employed to calculate differential track settlement. The model is constructed using a 2.5D Finite Element Method with Perfectly Matched Layers (FEM-PML) approach, and is solved in a hybrid fashion, encompassing both the frequency-wavenumber and time–space domains. This wavenumber finite element method is a computationally efficient method for the solution of three-dimensional domains. Two dimensions are solved via finite element theory while the third is solved analytically. It is therefore well-suited for 3D structures that can be approximated as having invariant geometry and material properties in one direction (e.g. railways, highways and tunnels). Assuming the structure is linear and elastic, the equations of motion can be solved in the wavenumber-frequency domain. A double Fourier transform is used to transform all variables into the wavenumber-frequency domain in terms of the moving direction of the train (x direction) and time (t). The main difference between the 2.5D and a 3D solution is that discrete sleepers can be simulated using 3D methods [23]. However, to approximate the reduced bending stiffness due to the presence of non-continuous sleepers, the 2.5D method uses modified anisotropy. The approach proposed by Alves Costa et al. [1] and Karlstrom and Bostrom [19] is used. The sleepers are modelled as continuous and orthotropic elements, incorporating the physical properties of the sleepers in the cross-section, with stiffness set to zero in the longitudinal plane. This approximation approach provides acceptable results within the investigated frequency range [20]. To capture all important waves within the frequency range of interest, the maximum wavenumber is constrained to 10 rad/m. Over the range from -10 to $+10$ rad/m, 1024 wavenumbers are sampled, a choice that effectively captures the peaks in the integrand while minimising computational complexity.

The two interconnected steps are visually presented in Fig. 1: Step A involves pre-calculating transfer functions, while Step B entails an iterative settlement process. Given the presence of repeated dynamic train loads, the proposed transfer function approach proves advantageous, as it enables the track geometry profile to be updated following each load passage with minimal computational burden. An investigation into the influence of track geometry update frequency on differential settlement was undertaken by Charoenwong, Connolly, Woodward, et al. [4]. Although updating after every axle passage is computationally demanding, failure to do so results in the incomplete capture of the effects of train-track interaction on differential settlement.

In Step A, a pre-calculation phase is undertaken, encompassing the calculation of the 3D elastodynamic response and geostatic stresses within both the track and the ground. The computation of the moving load transfer function, accounting for the non-linear track-ground stiffness, is executed within the frequency-wavenumber domain. Furthermore, the 3D stress transfer functions arising from quasi-static and dynamic loading conditions are derived, while several matrices necessary for the calculation of train-track dynamic interaction are also precomputed.

Step B involves an iterative solving procedure, which operates in both the wavenumber-frequency and space–time domains. Based on the track irregularity profile, track compliance, and rolling stock characteristics, the train-track dynamic interaction force is computed through a multi-body model. Subsequently, the overall stresses, encompassing quasi-static, dynamic, and geostatic components, along with settlements in both the track and the ground, are determined across the entire length of the model track, corresponding to the direction of train passage. Following each axle passage, the vertical track geometry profile undergoes updates, thereby necessitating the recalculating of both the train-track dynamic force and stresses at each iteration. These steps are repeated for the desired number of cycles, or until a threshold limit value, potentially specified by railway standards, is reached. It should be noted that due to the pre-calculations in Step A, Step B iteration only requires minimal computational resources, facilitating the rapid simulations of many axle passages. Additional information regarding the numerical model can be found in Charoenwong, Connolly, Woodward, et al. [4].

Train-track dynamic interaction

A comprehensive 2D vehicle model that incorporates the primary structural elements of train dynamics [37] is used for the rolling stock. The interaction between the vehicle and the track is addressed through a compliance method, applied using a dynamic frame of reference for the moving train [8,10]. The rolling-stock considered is a passenger train, formulated as a rigid multi-body vehicle with two levels of suspension as

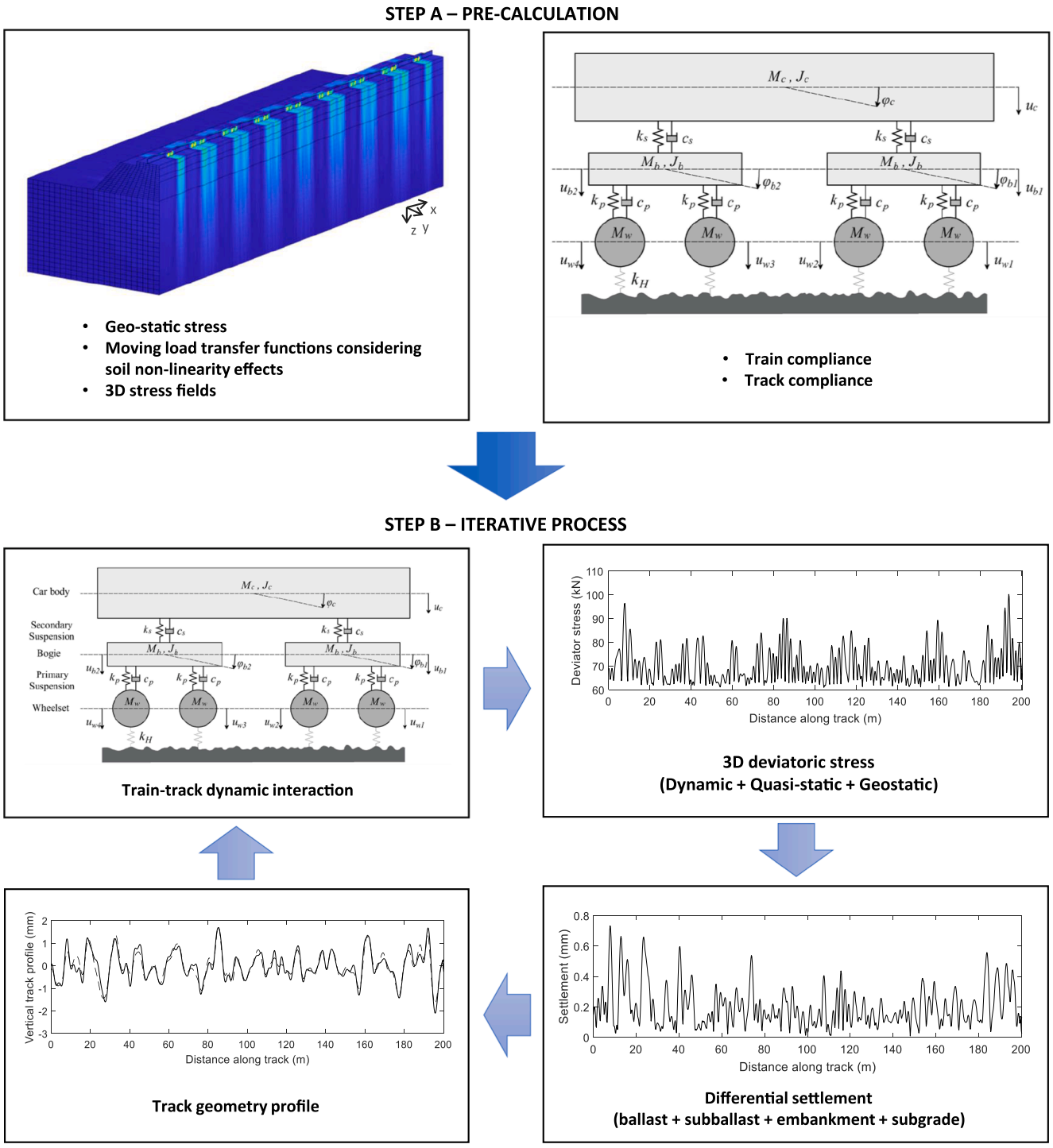

Fig. 1. Model overview.

shown in Fig. 2. In the context of differential settlement modelling, the errors associated with using simplified passenger vehicle models have been studied by Charoenwong, Connolly, Odolinski, et al. [3], where it is shown that a reduction of degrees of freedom results in unacceptable error levels. The analysis is carried out in the frequency domain, factoring in the conversion of the track profile from the spatial domain. Equations (1) to (7) provide the calculations for the dynamic interaction force in the frequency domain. When considering Hertzian stiffness, a linearization approach is employed where only the dead load transmitted by the wheelset is considered when deriving a representative value [21].

$$\{F_{dyn}(\Omega)\} = -\left([V] + [V^H] + [T]\right)^{-1}\{\Delta u(\Omega)\} \tag{1}$$

$$\{\Delta u(\Omega)\} = \delta u\{b(\Omega)\} \tag{2}$$

$$b(\Omega)_i = e^{i\frac{2\pi}{\lambda}a_i} \tag{3}$$

$$T(\Omega) = \frac{1}{2\pi}\int_{-\infty}^{+\infty} u_c^G(k_x,\omega)dk_x \tag{4}$$

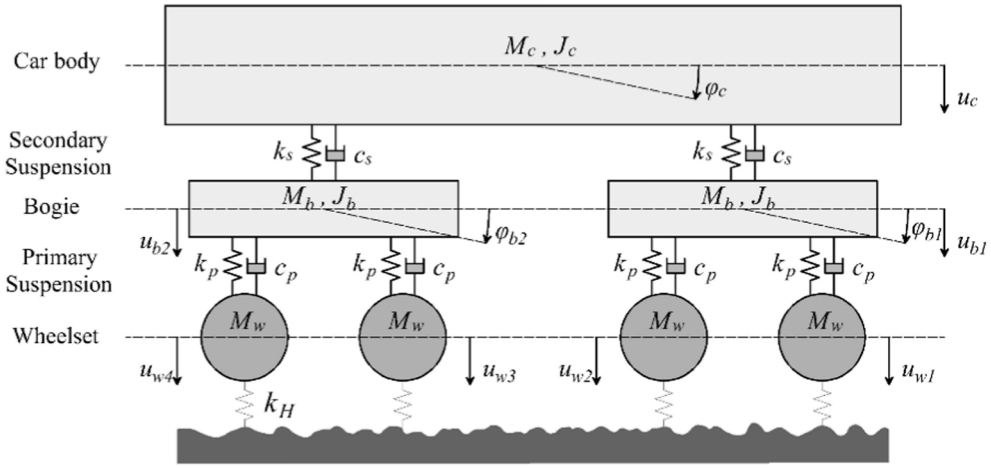

Fig. 2. Multi-body vehicle model.

$$V^H = \frac{1}{k_H} \tag{5}$$

$$k_H = \frac{3}{2G} P_0^{1/3} \tag{6}$$

$$V(\Omega) = [Z]\left([K^v] - \Omega^2[M^v]\right)^{-1}[Z]^T \tag{7}$$

$$[Z] = \begin{bmatrix} 0 & 0 & 0 & 0 & 0 & 0 & 1 & 0 & 0 & 0 \\ 0 & 0 & 0 & 0 & 0 & 0 & 0 & 1 & 0 & 0 \\ 0 & 0 & 0 & 0 & 0 & 0 & 0 & 0 & 1 & 0 \\ 0 & 0 & 0 & 0 & 0 & 0 & 0 & 0 & 0 & 1 \end{bmatrix} \tag{8}$$

In equations (1)–(7), Ω is the driving frequency, defined by $\Omega = \frac{2\pi}{\lambda} v_0$; T is the flexibility term of the track compliance; V is the flexibility term of the vehicle compliance; V^H is the contact flexibility matrix; k_H is the linearised (Hertzian) contact stiffness; P_0 is the static load transmitted by the wheel to the rail; G is the contact constant depending on the radius and geometry of the wheel, and rail bearing surface; Z is a constant matrix, M^v is the vehicle mass matrix and K^v is the vehicle stiffness. The mass and stiffness matrices of the vehicle system with primary and secondary suspensions can be found in Charoenwong, Connolly, Odolinski, et al. [3].

Regarding track irregularities, their profile can be characterised using power spectral density (PSD) based on spatial frequency, for which multiple formulations exist. In this study, the methodology proposed by the Federal Railway Administration (FRA) that classifies tracks into distinct categories to quantify their unevenness is adopted[13]. The formulation based on FRA is defined using the equations (9)–(11):

$$S_n(k_x) = \frac{A k_3^2 \left(k_x^2 + k_2^2\right)}{k_x^4 \left(k_x^2 + k_3^2\right)} \tag{9}$$

where the spatial frequency is $k_x = \frac{2\pi}{\lambda_{irr}}$, λ_{irr} is the wavelength of the irregularity, A is a roughness constant, and k_2 *and* k_3 are spatial frequency constants.

After computing the PSD, the amplitude of unevenness in terms of spatial frequency is:

$$\delta u_j = \left(\sqrt{2 S_n\left(k_{x_j}\right) \Delta k_x}\right) e^{-i\theta_j} \tag{10}$$

where Δk_x is the resolution retained for the spatial frequency, and θ is phase angle, taken as a random variable with uniform distribution in the range 0-2π. The metric considered for threshold exceedance is the standard deviation over a 200 m track length. The initial track profile in terms of position x is obtained using:

$$u_{irr}(x) = \sum_{j=1}^{N} \delta u_j e^{i k_{x_j} x} \tag{11}$$

Dynamic stresses along the track

When calculating differential settlement, stresses along the track in the direction of the train's movement are determined. The total stress includes geostatic stress, quasi-static stress, and dynamic stress. Both geostatic and quasi-static stresses are assumed to be constant along the track and can thus be computed in advance before the iterative train-track interaction process. However, dynamic stresses vary based on irregularities in track geometry and are updated with every iteration when the track geometry profile changes. To compute dynamic stresses along the railway track considering the full vehicle model, the subsequent steps are undertaken:

(1) Pre-calculate the unit load stresses $\sigma_{unit\_load}(\Omega, k_x)$ in the frequency Ω and wavenumber k_x domain. In this study, stresses are calculated every 0.2 m along the track length and at vertical depth intervals of 0.25 m.
(2) To minimise the run time during the calculation of dynamic stresses along the track within the iterative process, the unit load stresses $\sigma_{unit\_load}(\Omega, k_x)$ in the frequency Ω and wavenumber k_x domain are converted to the unit load stresses $\sigma_{unit\_load}(\Omega)$ in the frequency domain prior to the iterative process, using the following equation:

$$\sigma_{unit\_load}(\Omega) = \frac{1}{2\pi} \int_{-\infty}^{+\infty} \sigma_{unit\_load}(\Omega, k_x) dk_x \tag{12}$$

(3) Pre-calculate the variables $[V]$, $\left[V^H\right]$, $[T]$ and $b(\Omega)$ based on the chosen vehicle model.
(4) Use Equation (1) to calculate $F_{dyn\_1}(\Omega)$, $F_{dyn\_2}(\Omega)$, $F_{dyn\_3}(\Omega)$ and $F_{dyn\_4}(\Omega)$. These represent dynamic forces from the four wheels, with $\Delta u(\Omega)$ denoting the amplitudes of the updated track irregularity profile.
(5) Calculate dynamic stresses in the frequency domain based on the dynamic forces from the four wheels:

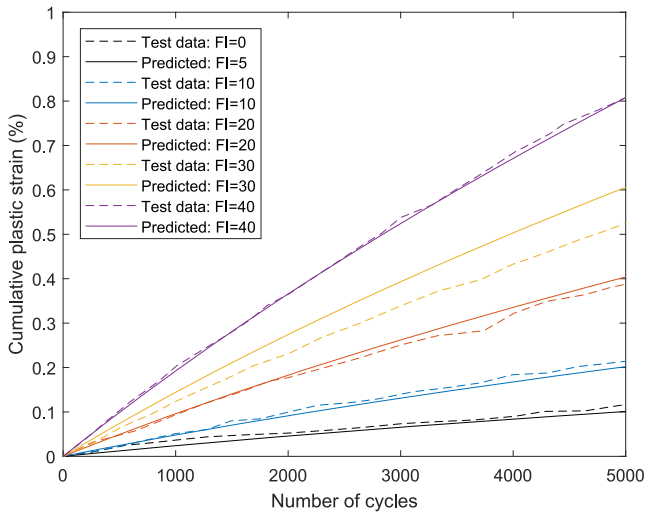

Fig. 3. Comparison of proposed ballast settlement model with experimental data for varying ballast fouling indices.

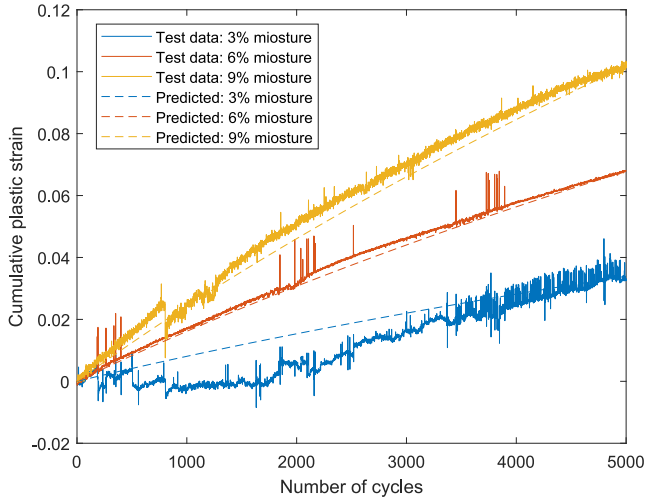

Fig. 4. Comparison of proposed ballast settlement model with experimental data, considering moisture of fines.

$$\begin{aligned}\sigma_{dyn\_1}(\Omega) &= \sigma_{unit\_load}(\Omega) \times F_{dyn\_1}(\Omega)\\ \sigma_{dyn\_2}(\Omega) &= \sigma_{unit\_load}(\Omega) \times F_{dyn\_2}(\Omega)\\ \sigma_{dyn\_3}(\Omega) &= \sigma_{unit\_load}(\Omega) \times F_{dyn\_3}(\Omega)\\ \sigma_{dyn\_4}(\Omega) &= \sigma_{unit\_load}(\Omega) \times F_{dyn\_4}(\Omega)\end{aligned} \tag{13}$$

(6) Before using the stresses to calculate settlement along the track, the four dynamic stresses in the frequency domain are transformed into the time–space domain using the following equation:

$$\begin{aligned}\sigma_{dyn\_1}(t) &= \sum_{j=1}^{N} \sigma_{dyn\_1}(\Omega_j) i\Omega_j t\\ \sigma_{dyn\_2}(t) &= \sum_{j=1}^{N} \sigma_{dyn\_2}(\Omega_j) i\Omega_j t\\ \sigma_{dyn\_3}(t) &= \sum_{j=1}^{N} \sigma_{dyn\_3}(\Omega_j) i\Omega_j t\\ \sigma_{dyn\_4}(t) &= \sum_{j=1}^{N} \sigma_{dyn\_4}(\Omega_j) i\Omega_j t\end{aligned} \tag{14}$$

Fouled ballast settlement model

Large-scale triaxial tests were performed by Qian et al. [31] using the University of Illinois Triaxial Ballast Tester. The investigation aimed to assess the influence of moisture on the mechanical performance of degraded ballast. It focused on analysing permanent deformation and shear strength attributes under varying moisture conditions, encompassing both dry and wet scenarios. The ballast was varied at FI levels: 0, 10, 20, 30, and 40, while the moisture content of the finer particles was varied at: 3 %, 6 %, and 9 %.

Based upon the test data, a model for ballast settlement is introduced, which takes into consideration both Ballast Fouling Index (*FI*) and moisture of fines (w). The new settlement equation is a modified version of that proposed by Li and Selig as shown in Eqs. (15) and (16) [26]. The coefficient A associated with plastic strain after the initial cycle of repeated loading is adapted to consider both ballast fouling and moisture. Additionally, it incorporates the ratio between the stress invariant quantity (t) and the Mohr–Coulomb failure criterion (t_{mc}) for a more universal/flexible approach that can be applied to all track layers. Considering the need to regularly update the track profile, the equation is also further refined to account for the settlement from previous axle passages in the build-up of plastic settlement, rather than simply consider the total number of cycles as is common in settlement modelling. This modification enables computation at each iterative step. This offers multiple benefits, for example being able to better capture the non-linearity of track settlement and greater flexibility in considering the rate of growth of track geometry (e.g. due to different magnitudes of axle loads [3]. The computation of permanent strain can be formulated as Eq. (17)., considering Eqs. (15) and (16):

$$\varepsilon_p = \overline{A} N^b \tag{15}$$

$$\overline{A} = \overline{a}\left(\frac{\sigma_d}{\sigma_s}\right)^m \tag{16}$$

where ε_p is the cumulative plastic strain (%); σ_d is the deviator stress; σ_s is the material static strength; $\overline{a}$, b and m are material constants for different soil types corresponding to clay content and soil plasticity as determined by Li [25].

$$\Delta\varepsilon_{p\_b,i} = ((w+1)\bullet c) \times (FI \bullet d) \times \left(\frac{t}{t_{mc}}\right)^a \times \left[\left(((dN \bullet i) + N_{lb})^b - 1\right) - \left(((dN \bullet (i-1)) + N_{lb})^b - 1\right)\right] \tag{17}$$

The corresponding settlement is then:

$$\Delta S_{b,i} = \sum_{j=1}^{k} \Delta\varepsilon_{p\_b,i_j} \bullet h_j \tag{18}$$

The term $\frac{t}{t_{mc}}$ defines the stress invariant quantity (t) and the Mohr–Coulomb failure criterion (t_{mc}) which can be calculated as follows:

$$t = \sqrt{2}\sqrt{J_2} \tag{19}$$

$$t_{mc} = \frac{\sqrt{2} sin\varnothing' s' + \sqrt{6} cos\varnothing' c'}{sin\theta sin\varnothing' + \sqrt{3} cos\theta} \tag{20}$$

Where θ is the lode angle, defined as:

$$\theta = -\frac{1}{3} sin^{-1}\left[\frac{3\sqrt{3}}{2}\left(\frac{J_3}{J_2^{3/2}}\right)\right] \tag{21}$$

Where J_2 and J_3 are the 2nd and the 3rd invariant of deviatoric stress, defined as:

$$J_2 = \frac{1}{6}\left[\left(\sigma_1' - \sigma_2'\right)^2 + \left(\sigma_2' - \sigma_3'\right)^2 + \left(\sigma_3' - \sigma_1'\right)^2\right] \tag{22}$$

$$J_3 = \left(\sigma_1' - \sigma_m'\right)\left(\sigma_2' - \sigma_m'\right)\left(\sigma_3' - \sigma_m'\right) \tag{23}$$

Where s' is the stress invariant quantity, defined as:

$$s' = \sqrt{3}\sigma_m' \tag{24}$$

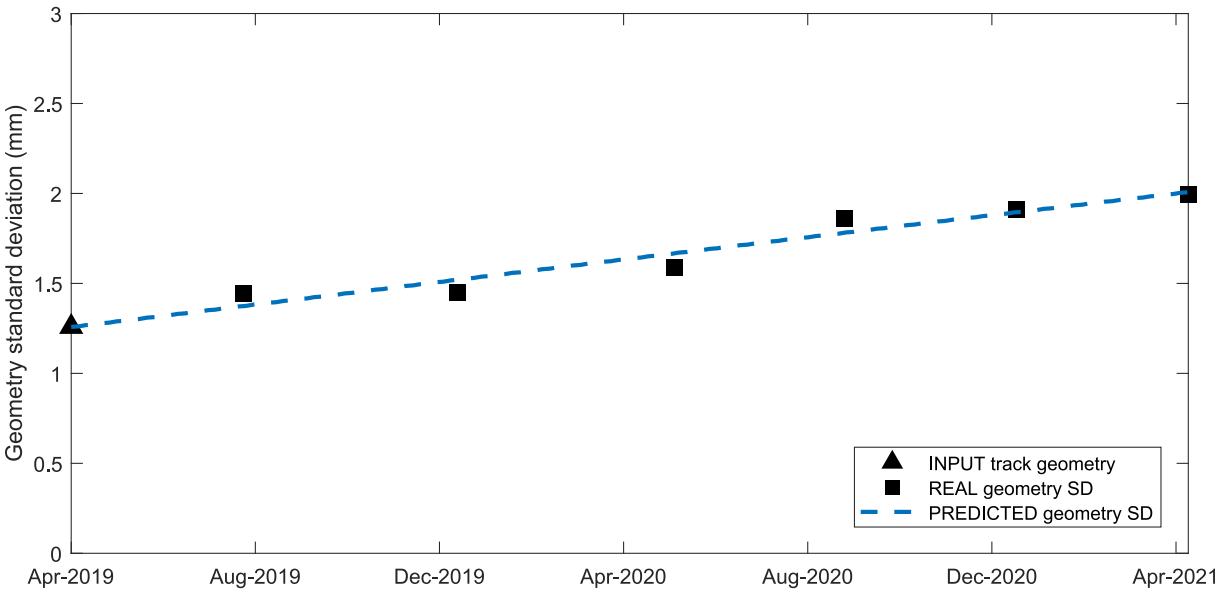

Fig. 5. Validation of vertical rail profile SD over time: predicted vs field data.

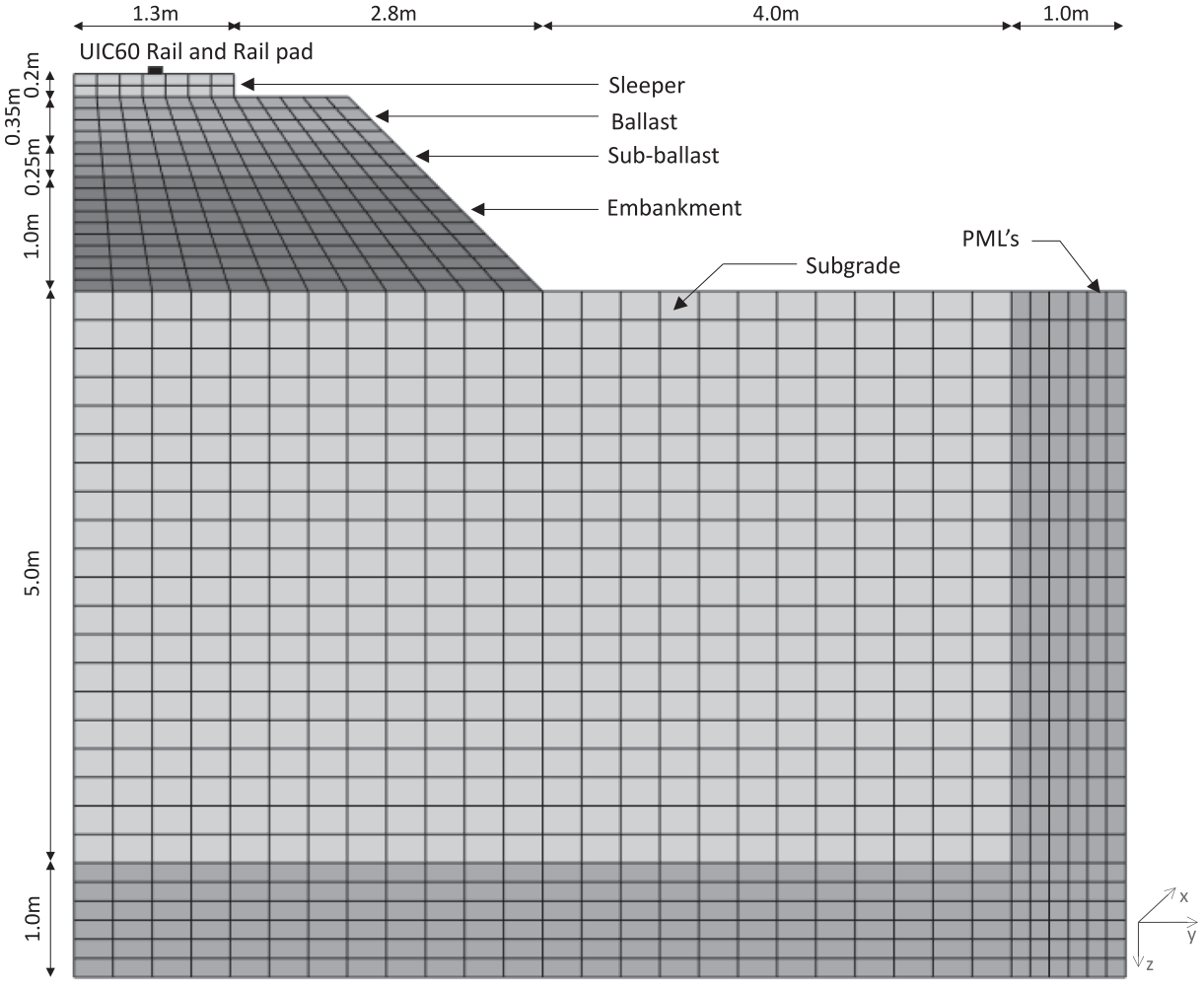

Fig. 6. Finite element mesh of ballasted track.

Table 1
Ballasted track properties.

Component	Parameter	Value
UIC 60 Rail (single rail)	Height (m)	0.172
	Length in transversal direction (m)	0.015
	Section area (m^2)	7.677×10^3
	Moment of Inertia y-y (m^4)	3.038×10^{-5}
	Moment of Inertia z-z (m^4)	0.512×10^{-5}
	Young's modulus (MPa)	2.11×10^5
	Density (kg/m^3)	7850
	Poisson's ratio	0.3
	Hysteresis damping coefficient	0.01
Railpad (spring element)	Continuous stiffness (N/m^2)	200×10^6
	Viscous damping (Ns/m^2)	22.5×10^3
Sleeper (G44)	Height (m)	0.2
	Length in transversal direction (m)	2.5
	Sleeper spacing (m)	0.65
	Young's modulus (MPa)	3×10^4
	Density (kg/m^3)	2500
	Poisson's ratio	0.2
	Hysteresis damping coefficient	0.01
Ballast	Height (m)	0.35
	Length in transversal direction (m)	2.8
	Young's modulus (MPa)	220
	Density (kg/m^3)	1600
	Poisson's ratio	0.12
	Hysteresis damping coefficient	0.06
Sub-ballast	Height (m)	0.25
	Length in transversal direction (m)	3.5
	Young's modulus (MPa)	210
	Density (kg/m^3)	2000
	Poisson's ratio	0.3
	Hysteresis damping coefficient	0.05
Embankment	Height (m)	1.0
	Young's modulus (MPa)	200
	Density (kg/m^3)	2000
	Poisson's ratio	0.3
	Hysteresis damping coefficient	0.05
	Shear wave speed (km/h)	706
Subgrade	Young's modulus (MPa)	70
	Density (kg/m^3)	2000
	Poisson's ratio	0.35
	Hysteresis damping coefficient	0.03

Where $\sigma_m^{'}$ is the mean effective stress, defined as:

$$\sigma_m^{'} = \frac{(\sigma_1^{'} + \sigma_2^{'} + \sigma_3^{'})}{3} \tag{25}$$

where $\Delta\varepsilon_{p\_b,i}$ is ballast permanent strain increment; i is iterative step; N_{lb} is the number of load cycles since the last ballast renewal/tamping; $\Delta S_{b,i}$ is ballast settlement increment; h_j is the thickness of each layer; k is number of sublayers; dN is the frequency of load application; FI is ballast fouling index (%) where $FI \geq 5 \,\&\, FI \leq 40$; w is moisture of fines (%) where $w \leq 9$; $\varnothing^{'}$ is friction angle; $c^{'}$ is cohesion; $\sigma_1^{'}$, $\sigma_2^{'}$, $\sigma_3^{'}$ are principal effective stresses; and a, b, c, d are empirical constants.

The model was fitted to the test data, as illustrated in Fig. 3 for ballast fouling index and Fig. 4 for moisture of fines. The empirical constants, represented as a, b, c and d, are: 2.15, 0.38, 0.013, and 0.0042, respectively. The proposed equation exhibits a good fit with the experimental data. However, it's important to acknowledge that the lowest value of FI employed in the proposed model is FI = 5, even though it originates from test data with FI = 0. This adjustment is necessary since it's challenging to substantiate the assumption that fresh ballast has a FI value of 0 in real-world scenarios.

Differential settlement model validation

The model's ability to predict the evolution of differential settlement with increasing axle passages is validated through comparison with historical track geometry data recorded using a track-recording-vehicle. An analysis is conducted on the standard deviation of the vertical track geometry profile spanning 200 m, focusing on wavelengths between 3 m and 35 m.

The material properties of the rails, rail pads, sleepers, ballast, sub-ballast, embankment, and subgrade are described in Appendix A. The subgrade properties are based upon site investigation data. The line operates with high freight traffic (60.49 % freight and 39.51 % passenger), and the assumed vehicle properties shown in Appendix B. The traffic volume per year is 25.24 million gross tonnes (MGT) with an operational linespeed of 100mph. To facilitate validation, track geometry obtained via a Track Recording Vehicle (TRV/TRC) on 7 dates from April 2019 to April 2021 is used. Analysis of maintenance records shows tamping was not performed between these dates.

The geometric data recorded in April 2019 serves as the starting track condition. Subsequently, the model simulates each axle load passage up to April 2021. The evolution of geometry SD is compared with the TRV data, illustrated in Fig. 5. The In-situ recorded geometry SD data is denoted by the black rectangular markers, while the red rectangular marker signifies the SD of the initial track profile in 2021. The red dashed line represents the predicted geometry SD, evolving after every axle passage. The strong correlation between the predicted geometry SD curve and the real data confirms the model is capable of predicting the evolution of differential track settlement.

Case studies

The model is used to perform four analyses. This section presents the track parameters including geometry conditions, and rolling-stock parameters.

Track parameters

The finite element mesh of the ballasted track is shown in Fig. 6. The track parameters including the characteristics of the rails, rail pads, sleepers, ballast, sub-ballast, embankment and subgrade properties are shown in Table 1.

Track geometry profile and traffic parameters

The initial track irregularity profile for both tracks is artificially generated using the PSD function [13], considering 40 frequencies. The values of parameters A, k_2 and k_3 are set as 0.043×10^{-6} $m^2 \bullet$ rad/m, 14.639×10^{-2} rad/m and 82.474×10^{-2} rad/m respectively, resulting in a track geometry profile with a starting standard deviation (SD) of 1.69 mm. It is intended that the initial track geometry falls within a definition of good track quality, suitable for a linespeed of 200 km/h. For both cases, it is assumed that the ballast has previously been subject to either traffic or dynamic track stabilisation to reduce the rapid initial rearrangement of ballast particles. The rolling stock is an Alfa Pendular passenger train operating at a linespeed of 200 km/h and the traffic volume is 25 million gross tons (MGT) per year. In order to replicate the long-term evolution of differential settlement, both case studies are subject to 25MGT of traffic per year and simulated for a period of three years.

Results

In this section, settlement behaviour considering varying Fouling Index (FI) ranging from 5 to 40 under dry subgrade conditions is presented. The degradation of track geometry, considering changing moisture content of fines (w = 3 %, 6 %, and 9 %) in heavily fouled

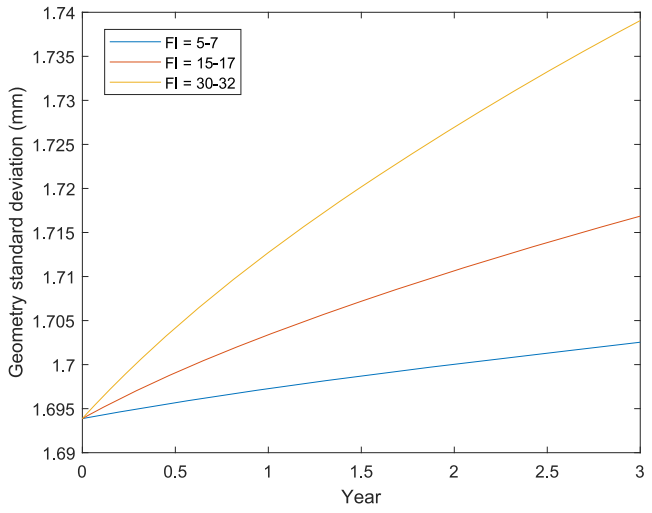

Fig. 7. Standard deviation evolution over time for varying ballast FI.

Table 2
Predicted SD after 3 years of traffic for varying ballast FI.

FI from year 1 to year 3	SD after 3 years of traffic in mm	SD increase in mm	Percentage increase
5 –> 7	1.7025	Baseline	0 %
15 –> 17	1.7169	0.0144	0.85 %
30 –> 32	1.7391	0.0366	2.15 %

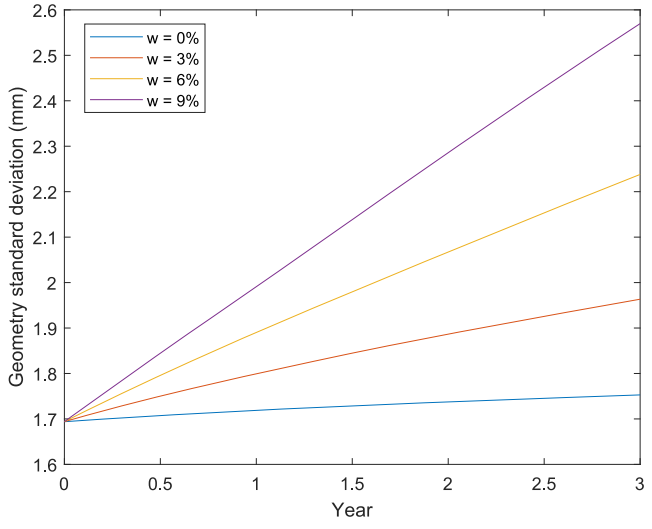

Fig. 8. Standard deviation evolution over time for varying moisture contents.

Table 3
Predicted SD after 3 years of traffic for varying moisture contents.

Moisture of fines in %	SD after 3 years of traffic in mm	SD increase in mm	Percentage increase
0	1.7528	Baseline	0 %
3	1.9634	0.2106	12.01 %
6	2.2379	0.4851	27.67 %
9	2.5698	0.8170	46.61 %

ballast is then studied. Additionally, the impact of reduced embankment stiffness (Ebm = 200 MPa and Ebm = 100 MPa) is explored across various levels of ballast FI and moisture content. Finally, the effect of altering line speed (100, 150, and 200 km/h) under different ballast conditions is analysed.

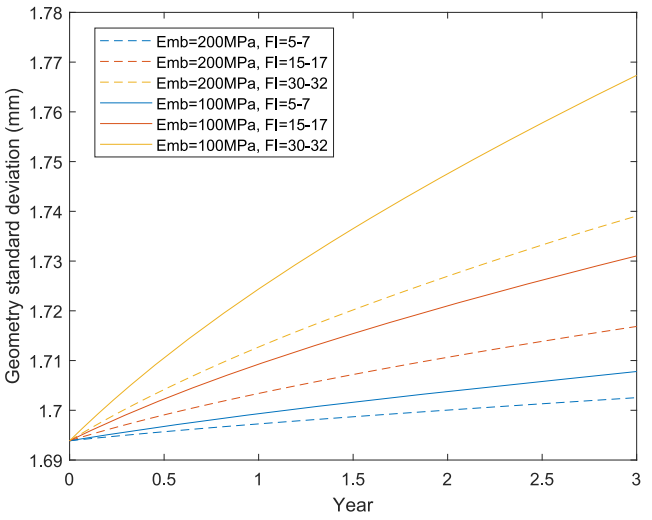

Fig. 9. Standard deviation evolution over time considering varying embankment stiffness and varying ballast FI.

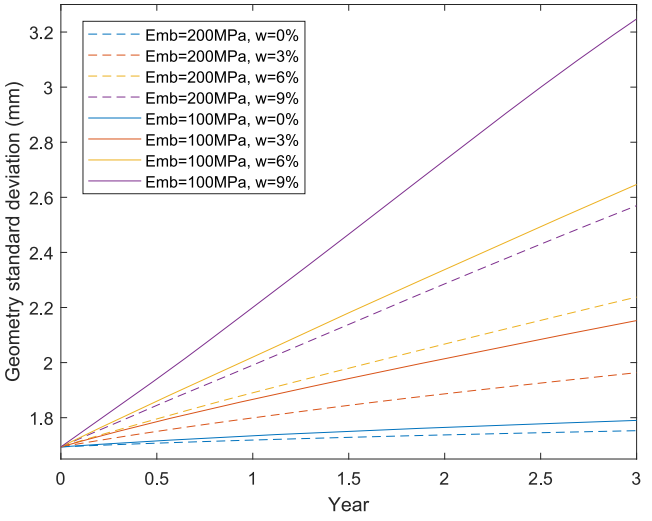

Fig. 10. Standard deviation evolution over time considering varying embankment stiffness for varying moisture contents.

Table 4
Predicted SD after 3 years of traffic considering varying embankment stiffness and varying ballast FI.

FI from year 1 to year 3	SD after 3 years of traffic in mm		Percentage increase
	Embankment E = 200 MPa (Baseline case)	**Embankment E = 100 MPa**	
5 –>7	1.7025	1.7078	0.31 %
15 –> 17	1.7169	1.7310	0.82 %
30 –>32	1.7391	1.7673	1.62 %

The effect of ballast fouling under dry subgrade conditions

Three dry scenarios are examined, involving variations of ballast FI from 5 to 40. These scenarios are defined as those with zero moisture of fines (0 %). The assumed rate of fouling generation resulting from ballast deterioration is 0.025 % per 1 MGT. Considering 3 years, the cumulative traffic is 75 MGT, representing an approximately 2 % rise in FI. For instance, an initial FI of 5 at the commencement of the first year is expected to gradually escalate to 7 by the end of the third year.

Fig. 7 compares the evolving geometry SD over time from the initial

Table 5
Predicted SD after 3 years of traffic considering varying embankment stiffness and varying moisture contents.

Moisture of fines %	SD after 3 years of traffic in mm		Percentage increase
	Embankment E = 200 MPa (Baseline case)	**Embankment E = 100 MPa**	
0	1.7528	1.7902	2.13 %
3	1.9634	2.1525	9.63 %
6	2.2379	2.6466	18.26 %
9	2.5698	3.2475	26.37 %

SD value in year 1 until year 3 for three different ranges of ballast FI. The corresponding SD after 3 years of traffic is summarised and compared in Table 2. The calculated SD after 3 years of traffic for initial FI values of 5, 15, and 30 are 1.7025 mm, 1.7169 mm, and 1.7391 mm, respectively. These values demonstrate that the deterioration of track geometry is not linear but rather accelerates with increasing ballast fouling. Using FI = 5 as the baseline, the predicted SD for starting FIs of 15 and 30 increases by 0.0144 mm and 0.0366 mm, corresponding to an increase of 0.85 % and 2.15 %, respectively. It is seen that the greater the initial fouling, the more pronounced the impact on track geometry.

The effect of moisture of fines

Continuing in a manner similar to the prior investigation, four scenarios are explored, but comparing varying levels of moisture of fines within heavily fouled ballast. The moisture content of fines considered are 0 %, 3 %, 6 %, and 9 %, with all scenarios being simulated at a constant ballast FI of 40.

Fig. 8 illustrates the evolving SD over a period from year 1 to year 3 for four distinct moisture content levels. The corresponding SD's after 3 years of traffic are summarised and compared in Table 3. The calculated SD after 3 years of traffic for moisture contents of 0 %, 3 %, 6 %, and 9 % are 1.7528 mm, 1.9634 mm, 2.2379 mm, and 2.5698 mm, respectively. The data clearly indicates that as the moisture content in the ballast increases, there is a significant escalation in the SD of track geometry. Using a moisture content of 0 % as the baseline, the predicted SD moisture of fines 3 %, 6 %, and 9 % is increased by 0.2106 mm, 0.4851 mm and 0.8170 mm, equating to 12.01 %, 27.67 %, and 46.61 %. These substantial percentage escalations demonstrate a progressive deterioration in track geometry with increasing moisture levels.

The effect of embankment stiffness

This section extends the investigation into the effects of embankment stiffness on settlement, considering varying levels of fouled ballast. To do so, the Young's modulus of the embankment is reduced from the baseline value of 200 MPa to a stiffness value of 100 MPa.

Figs. 9 and 10 illustrate the evolving SD over a period from year 1 to year 3 for three distinct FI and four distinct moisture content levels respectively. The corresponding SD's after 3 years of traffic are summarised and compared in Tables 4 and 5. Considering the low stiffness case, the predicted SD after 3 years of traffic for initial FI's of 5, 15, and 30 are 1.7078 mm, 1.7310 mm, and 1.7673 mm, corresponding to increases from the baseline case of 0.31 %, 0.82 %, and 1.62 %, respectively. Similarly, for moisture contents of 0 %, 3 %, 6 %, and 9 %, the predicted SDs after three years are 1.7902 mm, 2.1525 mm, 2.6466 mm, and 3.2475 mm, corresponding to an increase from the baseline case of 2.13 %, 9.63 %, 18.26 %, and 26.37 %, respectively. These results reveal a clear trend: reduced earthwork stiffness leads to increased SD values, especially at high moisture contents. Reduced stiffness earthworks tend to exacerbate the effects of both ballast fouling and moisture content, leading to more pronounced settlement over time.

Considering the worst-case scenario of a ballast FI of 40 and moisture content (w) of 9 %, Fig. 11(a) and 11(b) present the distribution of deviatoric stresses across the depths of the track-bed under quasi-static and dynamic excitations respectively. In these plots, the track-bed layers are defined as ballast, sub-ballast, and embankment. Observations indicate the reduced stiffness of the embankment influence the distribution of deviatoric stress within the track-bed. A stiffer embankment leads to an increase in deviatoric stresses within the embankment layer but a decrease in deviatoric stresses within the ballast layer. Specifically, within the ballast layer, the deviatoric stresses in the case of the reduced stiffness embankment are markedly higher compared to those in the baseline scenario. It should be noted that deviatoric stress (i.e. rather than solely vertical stress) is a key factor affecting settlement, with the majority of the settlement predominantly occurring within the ballast layer [2].

The effect of linespeed

Using the same track properties and initial track profile from the previous analyses, this section studies the impact of train speed on settlement, in the presence of fouled ballast. The investigation involves the simulations of three different speeds: 100, 150, and 200 km/h.

Fig. 12(a), 12(b), and 12(c) illustrate the evolving SD over a period from year 1 to year 3 for three speeds, each considering a different

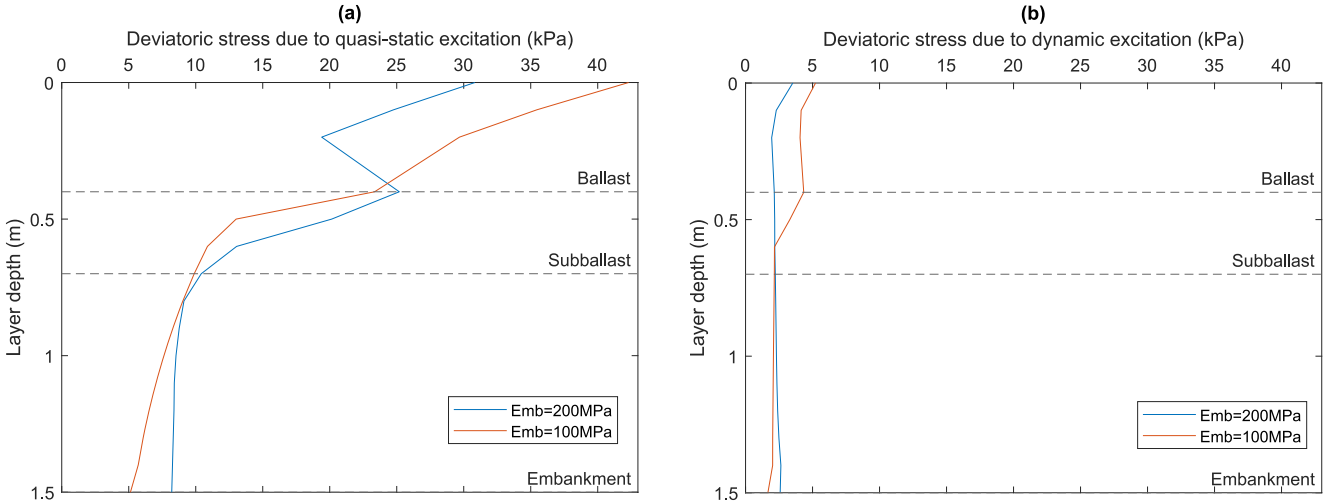

Fig. 11. Deviatoric stresses within the track-bed considering varying embankment stiffness: (a) quasi-static excitation (b) dynamic excitation.

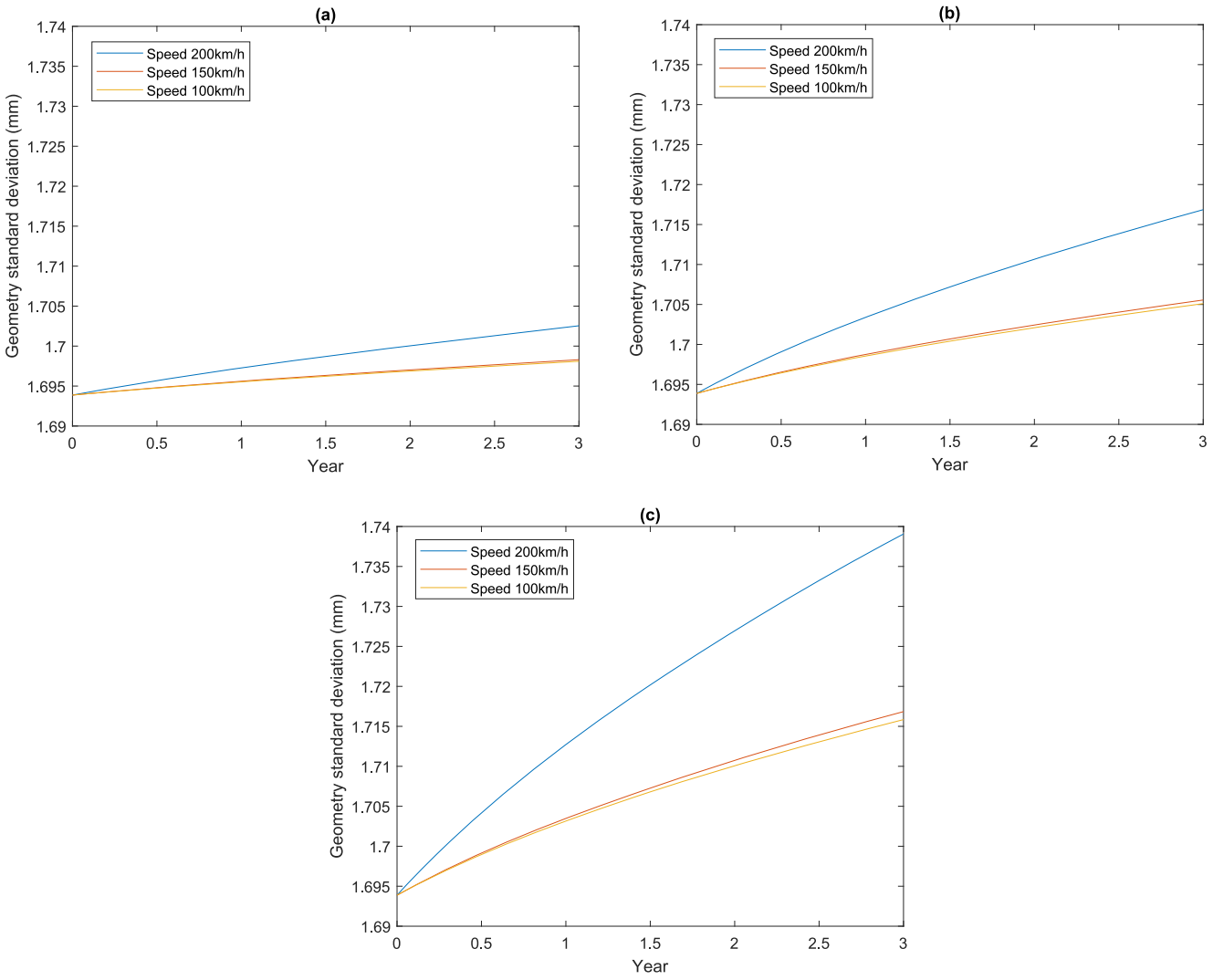

Fig. 12. Standard deviation evolution over time considering varying train speeds: (a) FI = 5 (b) FI = 15 and (c) FI = 30.

Table 6
Predicted SD after 3 years of traffic considering varying train speeds for varying ballast FI.

FI from year 1 to year 3	SD after 3 years of traffic in mm *(Percentage change)*		
	200 km/h	**150 km/h**	**100 km/h**
5 –> 7	1.7025 *(0.25 % increase)*	1.6983 *(Baseline)*	1.6981 *(0.01 % decrease)*
15 –> 17	1.7169 *(0.66 % increase)*	1.7056 *(Baseline)*	1.7051 *(0.03 % decrease)*
30 –> 32	1.7391 *(1.30 % increase)*	1.7168 *(Baseline)*	1.7158 *(0.06 % decrease)*

ballast FI. The corresponding SD's after 3 years of traffic are summarised and compared in Table 6. Using the speed of 150 km/h as a baseline case, it is found that for initial FI's of 5, 15, and 30, increasing the speed to 200 km/h results in SD increases of 0.25 %, 0.66 %, and 1.30 %, respectively. Conversely, reducing the speed to 100 km/h leads to decreases in SD of 0.01 %, 0.03 %, and 0.06 %, respectively. These results demonstrate that increased train speed results in higher track settlement. Specifically, when the speed is increased from 150 km/h to 200 km/h, there is a noticeable increase. This trend is consistent and escalates with higher FIs, suggesting that faster trains exert more stress on the track, exacerbating the settlement issues, particularly for fouled ballast conditions. While the reductions are relatively small, they indicate that slower train speeds marginally counteract the impact of ballast fouling on track settlement.

Similarly, Fig. 13(a), 13(b), and 13(c) demonstrate the SD evolution over the same period for varying train speeds, this time accounting for four different levels of moisture content. The corresponding SD's after 3 years of traffic are summarised and compared in Table 7. When the speed is increased from 150 km/h to 200 km/h, the SD rises by 1.68 %, 7.64 %, 15.16 %, and 22.95 %, respectively. Conversely, when the speed is decreased to 100 km/h, the SD reduces by 0.08 %, 0.45 %, 1.28 %, and 2.92 % for each respective moisture content level. These results are

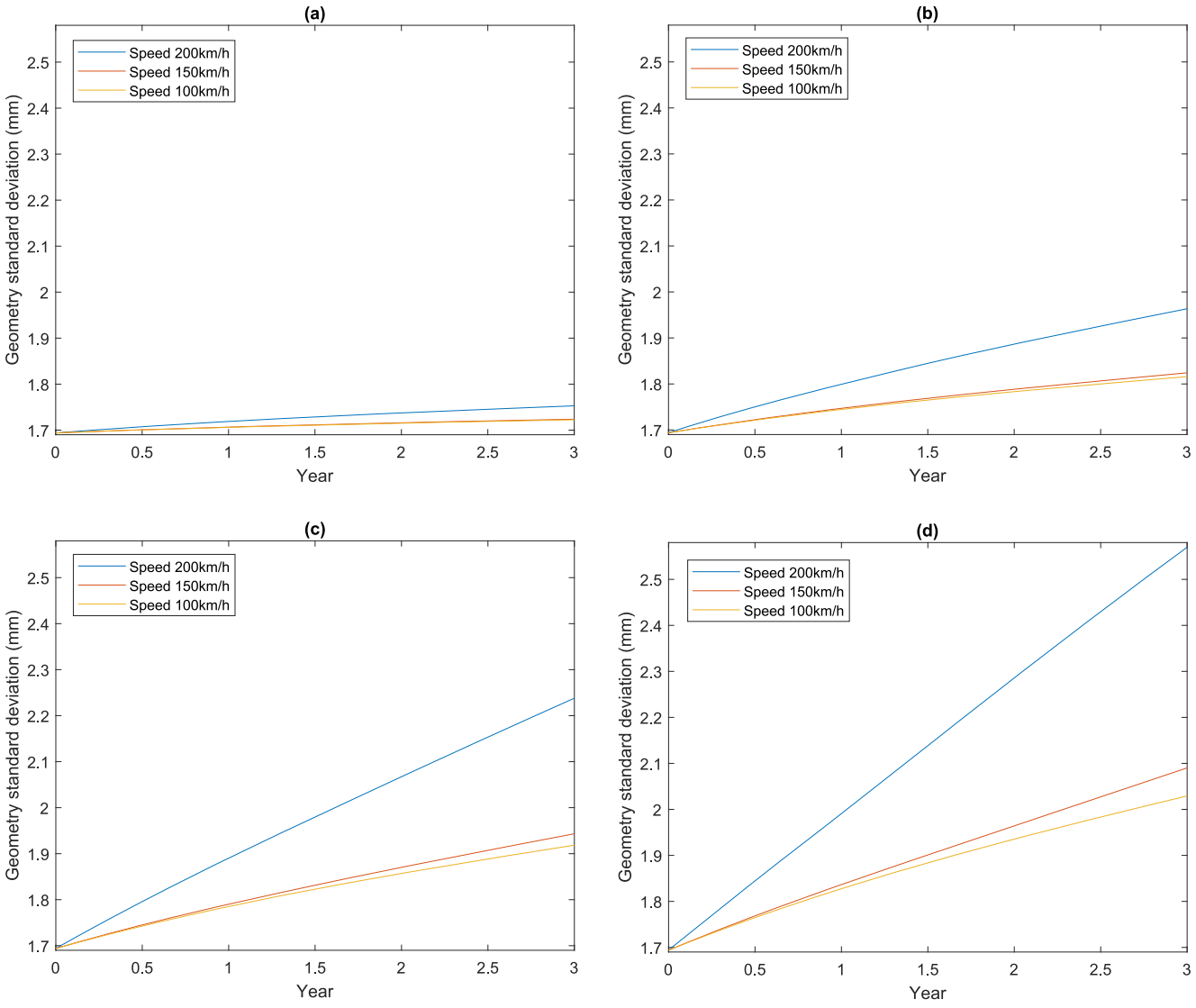

Fig. 13. Standard deviation evolution over time considering different train speeds: (a) w = 0 % (b) w = 3 % (c) w = 6 % and (d) w = 9 %.

Table 7
Predicted SD after 3 years of traffic considering different train speeds and varying moisture contents.

Moisture of fines %	SD after 3 years of traffic in mm *(Percentage change)*		
	Speed 200 km/h	**Speed 150 km/h**	**Speed 100 km/h**
0	1.7528 *(1.68 % increase)*	1.7238 *(Baseline)*	1.7225 *(0.08 % decrease)*
3	1.9634 *(7.64 % increase)*	1.8241 *(Baseline)*	1.8159 *(0.45 % decrease)*
6	2.2379 *(15.16 % increase)*	1.9433 *(Baseline)*	1.9184 *(1.28 % decrease)*
9	2.5698 *(22.95 % increase)*	2.0902 *(Baseline)*	2.0292 *(2.92 % decrease)*

consistent with the earlier trend: increasing the speed from 150 km/h to 200 km/h results in significant rises in SD. The substantial increases in SD with higher moisture contents at increased speeds highlight the compounded effect of moisture and speed on track settlement. Conversely, reducing the speed to 100 km/h leads to a reduction in SD.

Considering the scenario exhibiting the most pronounced effects (ballast FI is 40 and the moisture content (w) is 9 %), Fig. 14(a) and 14 (b) illustrate the distribution of deviatoric stresses throughout the depths of the track-bed under quasi-static and dynamic excitations, respectively. Observations indicate that a reduction in speed from 150 km/h to 100 km/h results in a slight decrease in deviatoric stresses caused by both quasi-static and dynamic excitations along the track-bed. Conversely, an increase in speed from 150 km/h to 200 km/h leads to a more significant escalation in deviatoric stresses, for both excitation types, compared to those observed at a speed of 100 km/h.

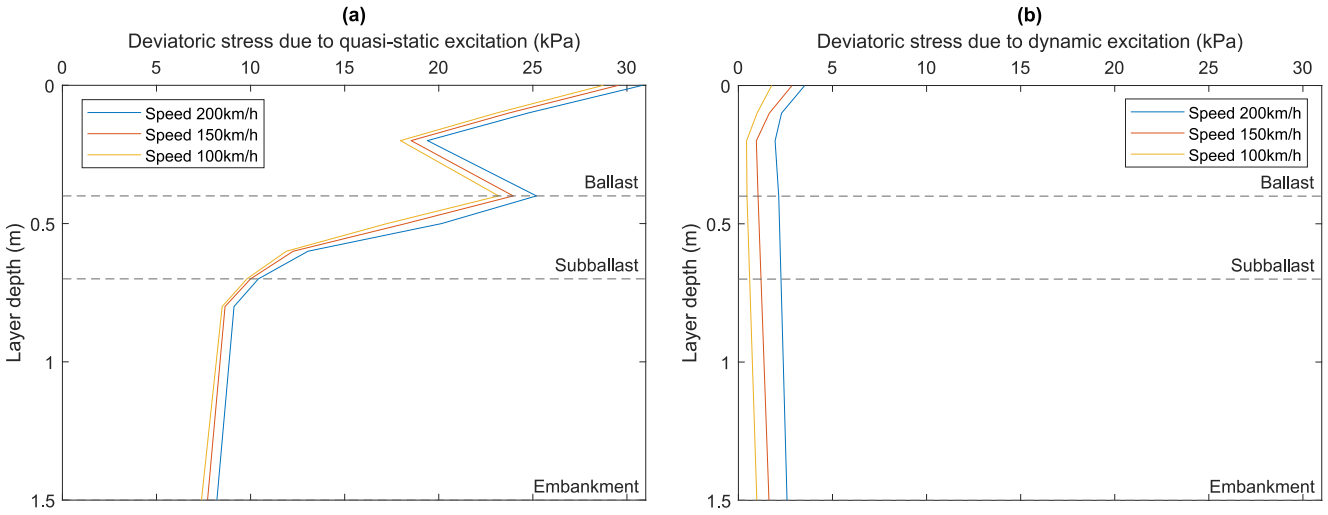

Fig. 14. Deviatoric stresses within the track-bed considering different train speeds: (a) quasi-static excitation (b) dynamic excitation.

Table 8
Correlation of Fouling Index, Moisture Content, and Settlement Rate.

Fouling index	Moisture content	Settlement rate
Low	Low	Low
Low	High	Site dependent
High	Low	Moderate
High	High	High

Discussion

It is evident that ballast moisture content and ballast fouling index have a linked effect on differential track settlement, as shown in Table 8. When the fouling index is low, water can flow freely through the ballast and can quickly exit the track. However, when fouling index is high, water drains more slowly and/or gets trapped in the ballast matrix. This can be effected depending upon whether the fouling material is primarily cohesive (e.g. from mud pumping) or granular (e.g. from ballast particle abrasion). Then in the presence of elevated water content there is greater scope for ballast particulates to rearrange, this leading to more rapid settlement. This is in contrast to the case of when fouling index is high but moisture content is low. In this scenario the fines have a limited effect on the rearrangement of ballast particles and any increases in settlement rate are marginal. The effects of fouling index and moisture content are magnified when the train speed is increased or the earthworks stiffness is low. This is because both scenarios lead to elevated deviatoric stresses within the ballast and supporting earthworks. This then induces increased settlement.

These findings underscore the importance of moisture management in maintaining track stability. Effective drainage and ballast quality are crucial to managing track geometry. Additionally, the track geometry should be kept in a condition suitable for the linespeed and the earthworks should give adequate support to the track. Note that in Table 8, the case of a low fouling index and high moisture content is classified as 'situation dependent'. This is because the presence of high levels of standing water, particularly if moving, can destabilise the ballast through the movement of stones, and erosion of the trackbed. This can result in rapid track settlement after the line is reopened and trains commence running at normal linespeed.

Conclusions

This paper presents a novel numerical algorithm, integrated with a new ballast settlement model, to predict differential track settlement in ballasted tracks, considering varying ballast moisture content and fouling levels. It takes into account the complexities of train-track interaction, vehicle dynamics, and the propagation of 3D stress fields, employing an equivalent-linear wavenumber finite element method to account for soil non-linearities experience in the high strain range. This approach allows for the evolution of track irregularities to be accurately modelled after each load passage. The validated model is used to perform four case studies, each related to different aspects affecting track settlement. The following conclusions are drawn:

1. Higher ballast fouling levels lead to faster deterioration in track geometry (differential settlement), particularly in the presence of moisture. When the ballast is heavily fouled and the moisture of fines is high, rapid deterioration occurs. In contrast, when the ballast is kept dry, the increase in degradation rate for fouled ballast is marginal.
2. Earthwork stiffness exacerbates the effects of ballast fouling and moisture content, leading to increased settlement when the earthworks are soft. This is in-part due to the distribution of deviatoric stress within the track-bed layers. In particular, the ballast layer shows a marked increase in stress in the presence of reduced embankment stiffness's;
3. Higher train speed increases differential settlement rate for all scenarios studied. However, the effect is low when the ballast has minimal fines and is kept dry. In contrast, when the ballast is heavily fouled and is subject to elevated levels of moisture, the track geometry degrades significantly faster when subject to higher speeds. This is because the higher train-track interaction forces at high speed induce elevated deviatoric stresses in the track, resulting in greater settlement because the elevated fines and moisture make it easier for the ballast particles to rearrange.

CRediT authorship contribution statement

C. Charoenwong: Writing – review & editing, Writing – original draft, Validation, Software, Methodology, Investigation. **D.P. Connolly:** Writing – review & editing, Writing – original draft, Supervision, Methodology. **P. Alves Costa:** Supervision. **P. Galvín:** Supervision. **A. Romero:** Supervision.

Declaration of competing interest

The authors declare that they have no known competing financial interests or personal relationships that could have appeared to influence the work reported in this paper.

Data availability

Data will be made available on request.

Acknowledgements

The authors wish to thank Dr Yu Qian for sharing the raw laboratory test data used to calibrate the settlement models and the financial support of the Leverhulme trust (PLP-2016-270).

Appendix A. Ballasted track properties (validation case)

Component	Parameter	Value
Rail (single rail)	Type	56E1
	Height (m)	0.159
	Length in transversal direction (m)	0.020
	Section area (m^2)	7.169×10^{3}
	Moment of Inertia y-y (m^4)	2.321×10^{-5}
	Moment of Inertia z-z (m^4)	0.422×10^{-5}
	Young's modulus (Pa)	2.11×10^{11}
	Density (kg/m^3)	7850
	Poisson's ratio	0.3
	Hysteresis damping coefficient	0.01
Railpad (spring element)	Continuous stiffness (N/m^2)	250×10^{6}
	Viscous damping (Ns/m^2)	22.5×10^{3}
Sleeper (G44)	Height (m)	0.2
	Length in transversal direction (m)	2.5
	Sleeper spacing (m)	0.65
	Young's modulus (Pa)	3×10^{10}
	Density (kg/m^3)	2500
	Poisson's ratio	0.2
	Hysteresis damping coefficient	0.01
Ballast	Height (m)	0.3
	Length in transversal direction (m)	3.2
	Young's modulus (Pa)	180×10^{6}
	Density (kg/m^3)	1600
	Poisson's ratio	0.25
	Hysteresis damping coefficient	0.06
Sub-ballast	Height (m)	0.25
	Length in transversal direction (m)	n/a
	Young's modulus (Pa)	210×10^{6}
	Density (kg/m^3)	2000
	Poisson's ratio	0.3
	Hysteresis damping coefficient	0.05
Embankment	Height (m)	1.0
	Young's modulus (Pa)	200 × 106
	Density (kg/m^3)	2000
	Poisson's ratio	0.3
	Hysteresis damping coefficient	0.05
	Shear wave speed (km/h)	706
Subgrade	Soil type	clay/silt
	Shear strength (kN/m^2)	150
	Young's modulus (Pa)	120×10^{6}
	Density (kg/m^3)	2000
	Poisson's ratio	0.35
	Hysteresis damping coefficient	0.03
	Shear wave speed (km/h)	692

Appendix B. . Vehicle properties

Parameter	Passenger	Freight
Number of cars	11	40
Number of axles	44	160
Axle spacing (m)	2.9	1.7
Bogie spacing (m)	19	9.7
Car body mass (kg)	329×10^2	864×10^2
Car body pitching moment of inertia (kg.m^2)	208×10^4	102×10^4
Bogie mass (kg)	4932	2800
Wheelset mass (kg)	1538	2000
Bogie pitching moment of inertia (kg.m^2)	5150	2020
Primary suspension stiffness (kNm^{-1})	3420	–
Primary suspension viscous damping (Nsm^{-1})	360 x10^2	–
Secondary suspension stiffness (kNm^{-1})	1320	2660
Secondary suspension viscous damping (Nsm^{-1})	360×10^2	25×10^2

References

[1] Alves Costa P, Calçada R, Silva Cardoso A, Bodare A. Influence of soil non-linearity on the dynamic response of high-speed railway tracks. Soil Dyn Earthq Eng 2010; 30(4):221–35. https://doi.org/10.1016/j.soildyn.2009.11.002.

[2] Charoenwong C, Connolly DP, Colaço A, Alves Costa P, Woodward PK, Romero A, et al. Railway slab vs ballasted track: A comparison of track geometry degradation. Constr Build Mater 2023;378:131121. https://doi.org/10.1016/j.conbuildmat.2023.131121.

[3] Charoenwong C, Connolly DP, Odolinski K, Alves Costa P, Galvín P, Smith A. The effect of rolling stock characteristics on differential railway track settlement: An engineering-economic model. Transp Geotech 2022;37:100845. https://doi.org/10.1016/j.trgeo.2022.100845.

[4] Charoenwong C, Connolly DP, Woodward PK, Galvín P, Alves Costa P. Analytical forecasting of long-term railway track settlement. Comput Geotech 2022;143: 104601. https://doi.org/10.1016/j.compgeo.2021.104601.

[5] Chen C, McDowell GR. An investigation of the dynamic behaviour of track transition zones using discrete element modelling. Proc Inst Mech Eng, Part F: J Rail Rapid Transit 2016;230(1):117–28. https://doi.org/10.1177/0954409714528892.

[6] Chumyen P, Connolly DP, Woodward PK, Markine V. The effect of soil improvement and auxiliary rails at railway track transition zones. Soil Dyn Earthq Eng 2022;155(December 2021):107200. https://doi.org/10.1016/j.soildyn.2022.107200.

[7] Chumyen P, Connolly DP, Woodward PK, Markine V. A comparison of earthwork designs for railway transition zones. Constr Build Mater 2023;395:132295.

[8] Colaço A, Costa PA, Connolly DP. The influence of train properties on railway ground vibrations. Struct Infrastruct Eng 2016;12(5):517–34. https://doi.org/10.1080/15732479.2015.1025291.

[9] Connolly DP, Costa PA. Geodynamics of very high speed transport systems. Soil Dyn Earthq Eng 2020;130(November 2019):105982. https://doi.org/10.1016/j.soildyn.2019.105982.

[10] Costa PA, Calçada R, Cardoso AS. Influence of train dynamic modelling strategy on the prediction of track-ground vibrations induced by railway traffic. Proc Inst Mech Eng, Part F: J Rail Rapid Transit 2012;226(4):434–50. https://doi.org/10.1177/0954409711433686.

[11] Dahlberg T. Some railroad settlement models - A critical review. Proc Inst Mech Eng, Part F: J Rail Rapid Transit 2001;215(4):289–300. https://doi.org/10.1243/0954409011531585.

[12] de Miguel A, Lau A, Santos I. Numerical simulation of track settlements based on an iterative holistic approach. J Braz Soc Mech Sci Eng 2018;40(8). https://doi.org/10.1007/s40430-018-1300-8.

[13] Federal Railroad Administration. (1980). *Statistical Representations of Track Geometry : Volume I.*

[14] Galvín P, Romero A, Domínguez J. Fully three-dimensional analysis of high-speed traintracksoil-structure dynamic interaction. J Sound Vib 2010;329(24):5147–63. https://doi.org/10.1016/j.jsv.2010.06.016.

[15] Grossoni I, Powrie W, Zervos A, Bezin Y, Le Pen L. Modelling railway ballasted track settlement in vehicle-track interaction analysis. Transp Geotech 2021;26 (August 2020):100433. https://doi.org/10.1016/j.trgeo.2020.100433.

[16] Guo Y, Zhao C, Markine V, Jing G, Zhai W. Calibration for discrete element modelling of railway ballast: A review. Transp Geotech 2020;23(January):100341. https://doi.org/10.1016/j.trgeo.2020.100341.

[17] Hasnayn MM, McCarter WJ, Woodward PK, Connolly DP. Railway subgrade performance after repeated flooding – Large-scale laboratory testing. Transp Geotech 2020;23:100329.

[18] Indraratna B, Nimbalkar S. Stress-strain degradation response of railway ballast stabilized with geosynthetics. J Geotech Geoenviron Eng 2013;139(5):684–700. https://doi.org/10.1061/(asce)gt.1943-5606.0000758.

[19] Karlström A, Boström A. An analytical model for train-induced ground vibrations from railways. J Sound Vib 2006;292(1–2):221–41. https://doi.org/10.1016/j.jsv.2005.07.041.

[20] Knothe K, Wu Y. Receptance behaviour of railway track and subgrade. Arch Appl Mech 1998;68(7–8):457–70. https://doi.org/10.1007/s004190050179.

[21] Kouroussis G, Connolly DP, Verlinden O. Railway-induced ground vibrations – a review of vehicle effects. Int J Rail Transport 2014;2(2):69–110. https://doi.org/10.1080/23248378.2014.897791.

[22] Kumar N, Kossmann C, Scheriau S, Six K. An efficient physical-based method for predicting the long-term evolution of vertical railway track geometries. Proc Inst Mech Eng, Part F: J Rail Rapid Transit 2021. https://doi.org/10.1177/09544097211024803.

[23] Lamprea-Pineda AC, Connolly DP, Castanheira-Pinto A, Alves-Costa P, Hussein MFM, Woodward PK. On railway track receptance. Soil Dyn Earthq Eng 2024;177:108331. https://doi.org/10.1016/j.soildyn.2023.108331.

[24] Lekarp, F., Isacsson, U., & Dawson, A. (2000). State of the art. II: Permanent strain response of unbound aggregates. *Journal of Transportation Engineering*, *126*(1), 76 – 83. 10.1061/(ASCE)0733-947X(2000)126:1(76).

[25] Li D. Railway track granular layer thickness design based on subgrade performance under repeated loading. Amherst, Mass: University of Massachusetts; 1994.

[26] Li D, Hyslip J, Sussmann T, Chrismer S. Railway geotechnics. CRC Press; 2015.

[27] Li D, Selig ET. Resilient modulus for fine-grained subgrade soils. J Geotech Eng 1994;120(6):939–57.

[28] Li D, Selig ET. Cumulative plastic deformation for fine-grained subgrade soils. J Geotech Eng 1996;122(12):1006–13. https://doi.org/10.1061/(asce)0733-9410(1996)122:12(1006).

[29] Menan Hasnayn M, John McCarter W, Woodward PK, Connolly DP, Starrs G. Railway subgrade performance during flooding and the post-flooding (recovery) period. Transp Geotech 2017;11:57–68. https://doi.org/10.1016/j.trgeo.2017.02.002.

[30] Nielsen JCO, Li X. Railway track geometry degradation due to differential settlement of ballast/subgrade – Numerical prediction by an iterative procedure. J Sound Vib 2018;412:441–56. https://doi.org/10.1016/j.jsv.2017.10.005.

[31] Qian Y, Tutumluer E, Hashash YMA, Ghaboussi J. Triaxial testing of new and degraded ballast under dry and wet conditions. Transp Geotech 2022;34 (February):100744. https://doi.org/10.1016/j.trgeo.2022.100744.

[32] Ramos A, Gomes Correia A, Indraratna B, Ngo T, Calçada R, Costa PA. Mechanistic-empirical permanent deformation models: Laboratory testing, modelling and ranking. Transp Geotech 2020;23(January). https://doi.org/10.1016/j.trgeo.2020.100326.

[33] Selig ET, Waters JM. Track geotechnology and substructure management. In *University of Massachusetts USA;* 1994. 10.1680/tgasm.20139.

[34] Shan Y, Zhou S, Zhou H, Wang B, Zhao Z, Shu Y, et al. Iterative method for predicting uneven settlement caused by high-speed train loads in transition-zone subgrade. Transp Res Rec 2017;2607:7–14. https://doi.org/10.3141/2607-02.

[35] Shih JY, Grossoni I, Bezin Y. Settlement analysis using a generic ballasted track simulation package. Transp Geotech 2019;20(May):100249. https://doi.org/10.1016/j.trgeo.2019.100249.

[36] Thom NH, Brown SF. Effect of moisture on the structural performance of a crushed-limestone road base. Transp Res Rec 1987:50–6. https://www.scopus.com/inward/record.uri?eid=2-s2.0-0023591151&partnerID=40&md5=51ee7875f66d51198e476de2b2865498.

[37] Zhai W, Cai Z. Dynamic interaction between a lumped mass vehicle and a discretely supported continuous rail track. Comput Struct 1997;63(5):987–97. https://doi.org/10.1016/S0045-7949(96)00401-4.